Phase Correlation and Linewidth Reduction of 40 GHz Self-Pulsation in Distributed Bragg Reflector Semiconductor Lasers

Jeremie Renaudier, Guang-Hua Duan, *Senior Member, IEEE*, Pascal Landais, *Member, IEEE*, and Philippe Gallion, *Senior Member, IEEE*

***Abstract*—In this paper, self-pulsation (SP) in a distributed Bragg reflector (DBR) semiconductor laser without a saturable absorber is experimentally and theoretically investigated. Detailed experimental characterizations of the SP DBR laser are reported in the optical and radio-frequency domains. Phase correlation between the longitudinal modes selected by the DBR mirror has been experimentally demonstrated. A theoretical model based on coupled rate equations for three modes has been developed to study the time evolution of phases and amplitudes of the modes. The carrier density modulation, resulting from the beating between adjacent longitudinal modes generates four-wave mixing (FWM) and is responsible for mutual injection locking, leading to passive mode-locking. The calculated power spectral density of the frequency noise derived from the model is in agreement with experimental results and proves that the phases of the longitudinal modes are identically correlated through the FWM process in this type of SP lasers.**

***Index Terms*—Distributed Bragg reflector (DBR) lasers, mode-locked lasers, optical mixing, phase synchronization, pulsed lasers.**

I. Introduction

In order to improve transmission distance, transparency, capacity and speed of optical networks, much attention has been paid to investigating practical means for all-optical signal processing, for example all-optical digital logic functions and retiming, reshaping and reamplifying (3R) regenerators [1], [2]. All-optical clock recovery regeneration at 40 Gbit/s and beyond appears to be a crucial element for future transparent networks. One solution to achieve the regeneration is an all-optical clock recovery element combined with a Mach–Zehnder interferometer [2]. In this respect truly all-optical clock recovery is of very high interest as it would supersede the complicated optoelectronic schemes including: a high speed photo-receiver, a high-Q filter, a power amplifier, and a high speed laser or an integrated laser modulator. Among the different approaches investigated so far, we can mention in particular the one using self-pulsating (SP) lasers.

SP is a periodic variation of the output power of the laser even though it is dc biased. For instance, SP has been observed in Fabry–Perot (FP) [3], [4], distributed feedback (DFB) [5], [6] and distributed Bragg reflector (DBR) [7], [8] semiconductor lasers. The SP FP laser is not convenient for all-optical clock recovery applications, as the wavelength of the recovered clock would be the same as that of the input data. Alternatively, SP DFB lasers with several configurations have been demonstrated for all-optical clock recovery: phase-comb [5], [9], active mirror [10], and gain-coupled [6], [11]. Both phase-comb and gain-coupled SP DFB lasers contain two sub-DFB sections and a phase section. Each sub-section has a specific corrugation step. SP originates from the beating between two longitudinal modes co-existing in the cavity. However, these types of SP laser are quite complex in terms of fabrication process and behavior.

The other option is the DBR-type laser structure. There are two types of SP DBR lasers: with [7], [12] and without a saturable absorber [8], [13]. In DBR lasers with a saturable absorber, SP originates from the modulation of the absorption. The nonlinearities and characteristic times of semiconductor devices lead to oscillation at frequencies up to 500 GHz in this type of DBR lasers [7]. In DBR lasers without a saturable absorber, the beating between the longitudinal modes generates a power oscillation under appropriate bias conditions. All-optical clock recovery at 40 Gbit/s [12], [13] and 160 Gbit/s [8] has been demonstrated with both types of SP DBR structure. However, no detailed experimental characteristics of SP DBR without a saturable absorber has been published so far. From the theoretical point of view, although it was suggested that the four-wave mixing (FWM) is the origin of SP in such DBR lasers [14], [15], a quantitative description of phase correlation and linewidth reduction in this type of SP laser is still lacking.

The aims of this paper are 1) to report detailed characteristics of SP in a DBR without a saturable absorber; and 2) to investigate theoretically and experimentally the phase correlation and linewidth reduction in such components. The paper is organized as follows. Section II describes the laser structure and SP performance achieved. Section III is devoted to experimental characterization of the phase correlation between the longitudinal modes. Section IV develops the model, taking into account the evolution of the amplitude and the phase of the complex electric field of each longitudinal mode. From this model, the phase correlation of these modes is calculated. A discussion on the linewidth reduction is given in Section V.

Manuscript received July 11, 2006; revised September 14, 2006. This work was supported in part by the French RNRT "ROTOR" project and in part by the Science Foundation Ireland "05/RFP/ENG0040" project.

J. Renaudier was with the Alcatel Thales III-V Laboratory, 91767 Palaiseau, France and with the Ecole Nationale Supérieure des Télécommunications, CNRS LTCI, UMR 5141, 75634 Paris Cedex 13, France. He is now with Alcatel Research & Innovation, 91470 Marcoussis, France.

G.-H. Duan is with the Alcatel Thales III-V Laboratory, 91767 Palaiseau, France.

P. Landais is with the School of Electronic Engineering, Dublin City University, Dublin 9, Ireland.

P. Gallion is with the Ecole Nationale Supérieure des Télécommunications, CNRS LTCI, UMR 5141, 75634 Paris Cedex 13, France.

Digital Object Identifier 10.1109/JQE.2006.886820

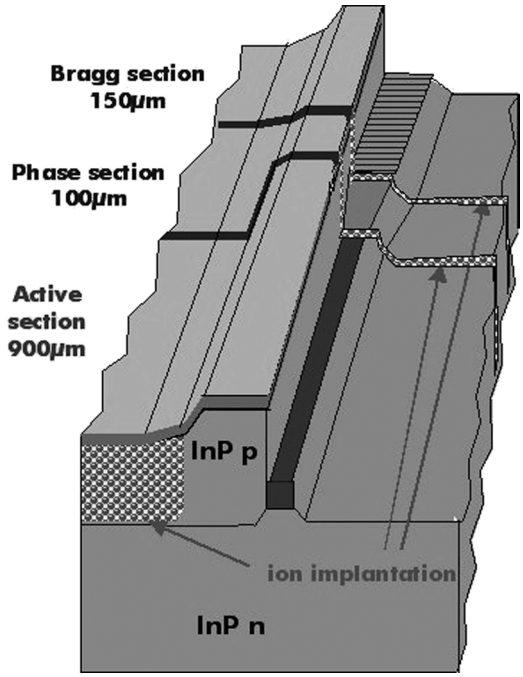

Fig. 1. Schematic of the SP DBR laser.

II. Laser Description and Characterization

Typical DBR lasers without saturable absorbers which are designed to self-pulsate, consist of active, phase and Bragg sections as depicted in Fig. 1. The particularity of SP DBR lasers, compared to those designed for other applications such as tunability, is to operate in the multimode regime. Consequently, we studied SP DBR lasers with a short Bragg section of 150 μm leading to a spectral linewidth of the main lobe of 5 nm. Such a broad reflectivity bandwidth allows to have at least three longitudinal modes of 40-GHz mode-spacing with comparable output power (power ratio between modes larger than 10%) in the emission spectrum. The active section is 900 μm long and consists of nine quantum wells and eight barriers 8 and 10 nm thick, respectively, surrounded by two separated confinement heterostructure guiding layers of total thickness of 200 nm. A 1.5-μm-wide waveguide ensures single-transverse-mode behavior of the electric field. The phase section is 100 μm long, with a waveguide width expanding linearly up to the 1.8-μm width of the Bragg section. This section adapts the optical modes between both the active and passive optical waveguides. It is kept unbiased for all experiments reported in this article since it is only used for fine-tuning the emitted wavelength. The different sections are electrically isolated ($\sim$ 1 $M\Omega$) by ion implantation. The injected currents in the active and Bragg sections are called I_a and I_b, respectively. Under broad bias conditions, such a DBR laser operates typically in a multimode regime allowing for the existence of SP by longitudinal modes beating. To characterize SP in DBR lasers, the output light was collected by a single mode fiber with an isolator (>70 dB) to avoid feedback, and was then sent to a slow response power meter, an optical spectrum analyzer and a 50-GHz band-pass photodiode followed by an electrical spectrum analyzer (ESA), with a resolution bandwidth fixed to 300 kHz. Fig. 2 shows an example of multimode optical spectrum emitted by such a laser for a driving dc active current of 150 mA. The other sections are not biased. This optical spectrum clearly reveals that the laser operates with three dominant longitudinal modes separated by about 0.32 nm, using a resolution bandwidth of 0.07 nm. The beating between these modes generates SP at the mode-spacing frequency given by the following expression:

$$\nu_{\rm sp} = \frac{c}{2(n_g L_a + n_\varphi L_\varphi + n_B L_{\rm eff})}$$

where c is the velocity of light, L_a, L_φ, and $L_{\rm eff}$ are the active, phase and effective lengths [16] respectively, n_g, n_φ, and n_B their associated group indices. Fig. 3 shows an example of the electrical spectrum of the photocurrent observed at the same bias condition as for Fig. 2. A Lorentzian lineshape centered on a frequency close to 39.5 GHz, with a full width at half-maximum of approximately 800 kHz approximately can be observed. This SP frequency corresponds to the 0.32-nm mode-spacing between the longitudinal modes measured directly from Fig. 2.

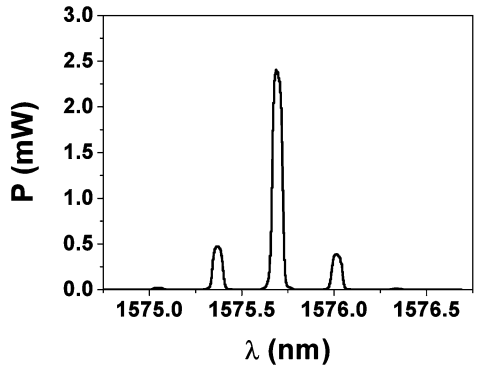

Fig. 2. Typical optical spectrum measured for an injected active current of 150 mA.

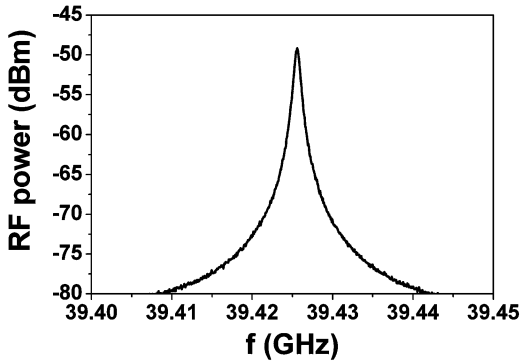

Fig. 3. Measured radio frequency spectrum corresponding to the optical spectrum shown in Fig. 2.

Fig. 4 shows the evolutions of the output power and of the wavelength of the main optical mode as a function of the driving active current, with unbiased Bragg section. The threshold current of such a laser is $\sim$15 mA, and power saturation due to thermal effects occurs at $\sim$250 mA. We can see on this figure the typical phenomenon of mode hopping in DBR lasers, where the magnitude of each mode jump corresponds to the mode-spacing. The evolution of the SP frequency versus the active current is

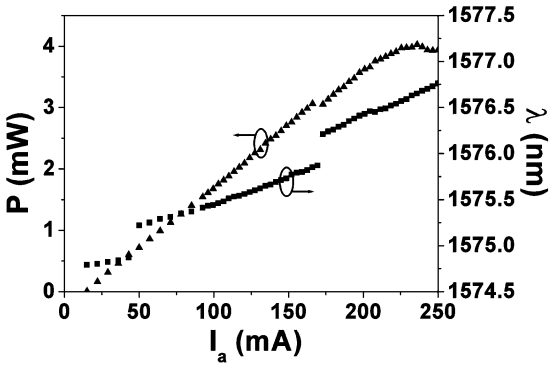

Fig. 4. Output power and wavelength of the main optical mode evolutions as functions of the active current with unbiased Bragg section.

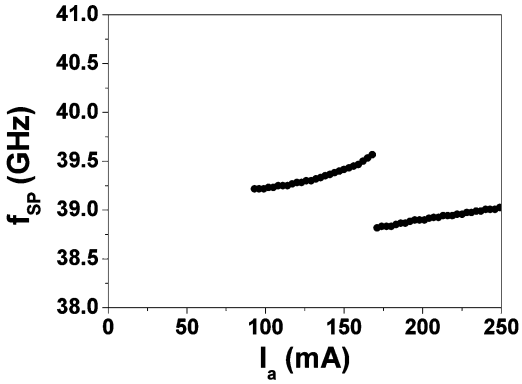

Fig. 5. SP frequency evolution versus the active current with unbiased Bragg section.

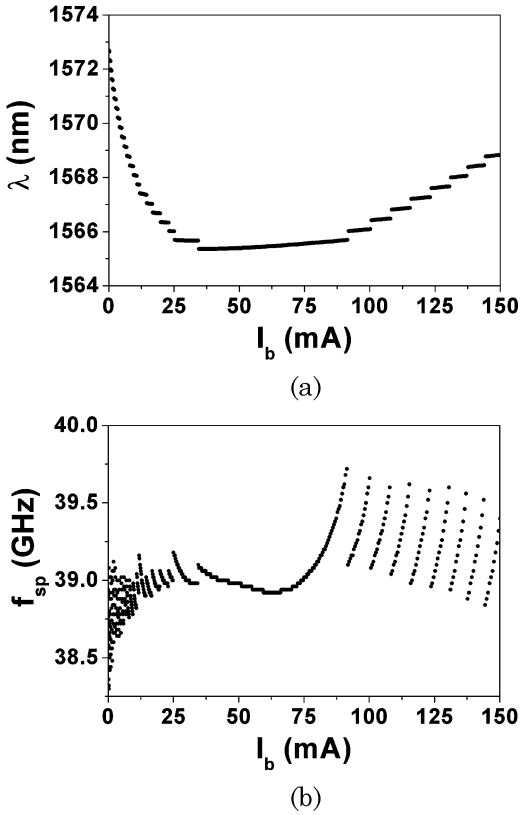

Fig. 6. Evolutions of (a) the wavelength of the main optical mode and (b) of the SP frequency as functions of the Bragg current, with an active current of 200 mA.

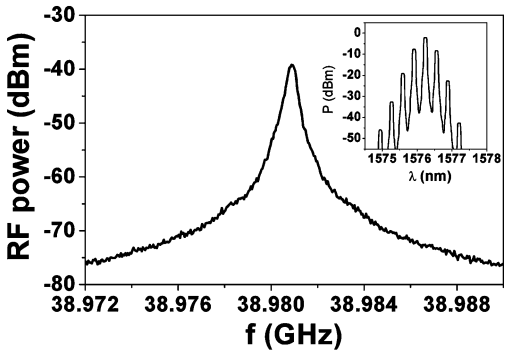

Fig. 7. Radio frequency spectrum of the DBR laser at the operating point. The insert is the corresponding optical spectrum.

shown in Fig. 5. SP occurs continuously for a large range of injected active currents above 90 mA. It seems that SP is likely to be established as soon as the active current reaches 90 mA, which corresponds only to six times the threshold current. Such a result indicates that the nonlinear effects responsible for SP arise for a small power level in the DBR lasers. Moreover, we can see a SP frequency jump for an injected current of 170 mA. Such a jump in the frequency curve is the consequence of mode hopping phenomenon, as shown in Fig. 4.

Fig. 6(a) and (b) presents the tunability of the wavelength of the main mode and of the SP frequency as a function the Bragg current, with an active current of 200 mA. As described in [17], current injection in the Bragg section enables the change of refractive index, either by plasma effect or by thermal effect, leading to both dominant wavelength and SP frequency shifts. The wavelength and SP frequency tunabilities for a given active current of 200 mA are measured at 8 nm and 1 GHz, from figures Fig. 6(a) and (b), respectively. Therefore, the control of the active and the Bragg currents can provide tunability over a range of 10 nm and 1 GHz, which is convenient for 40-Gbit/s all-optical clock recovery application.

III. Experimental Demonstration of Phase Correlation Between Longitudinal Modes

To understand the properties of the observed SP phenomenon, a detailed study is then focused on a fixed operating point: the active current is set to 200 mA and the Bragg and phase sections are kept unbiased. With the same experimental setup as used in Part 2, the radio-frequency (RF) spectrum of the photocurrent is measured and displayed in Fig. 7. In this measurement, the ESA was set to a 18-MHz span and a 300-kHz resolution bandwidth. The photocurrent exhibits a Lorentzian shape at a frequency of 39 GHz approximately. The measured spectral linewidth at half maximum of this RF signal is about 700 kHz. The optical spectrum at this operating point is also shown in the insert. The laser operates in a three-mode regime: the strongest is labelled number 2, and the next modes, respectively, on the right and on the left are labelled number 1 and number 3 as shown in Fig. 8. The other modes, at least 10 dB

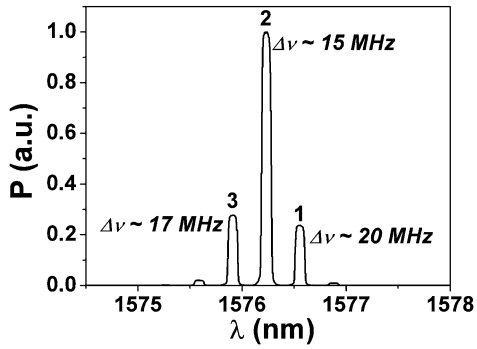

Fig. 8. Measurement of the linewidths of the optical modes for an active current of 200 mA.

lower in power than the third one, have negligible contributions to the SP phenomenon observed. The longitudinal modes are individually selected by a 0.1-nm band-pass filter and their spectral linewidths are measured using a self-heterodyne technique based on a Mach–Zehnder interferometer. The measured linewidths vary from 15 to 20 MHz between the dominant mode (2) and the lowest one (1) and are reported on Fig. 8. Comparing these values to that of the SP signal measured on the ESA, the RF signal from SP is largely narrower than the longitudinal modes, as in FP semiconductor lasers [4]. Although the phase of each longitudinal mode fluctuates upon spontaneous emission, the reduced linewidth of the SP signal shows that these fluctuations are largely synchronized. Such a linewidth reduction is actually the experimental signature of SP in DBR lasers without a saturable absorber.

To go further in our experiment, the two beat notes (e.g., between modes 1 and 2 and between modes 2 and 3) at the mode-spacing frequency that constitute the SP signal are separated. The coupled output light is now led to a monochromator, which acts as an optical tunable band-pass filter. Setting the filtering band-pass to 0.5 nm, the monochromator enables the selection of two optical modes. Then, the filtered optical signal is directly led to the photodiode followed by the ESA to characterize the two-mode beating. Fig. 9(a) displays the RF spectrum of the photocurrent representing the beat note between modes 1 and 2. The insert represents the optical spectrum of modes 1 and 2 filtered by the monochromator. The RF spectrum also appears as a Lorentzian-shaped signal, whose maximum power is largely reduced compared to that of Fig. 7. This 25 dB reduction corresponds roughly to the power losses due to the optical filtering. The measured spectral linewidth at half maximum is about 710 kHz, which is close to the spectral linewidth of the entire SP signal. Similarly, the RF spectrum representing the beat note of modes 2 and 3 is shown in Fig. 9(b) and the insert shows the corresponding filtered optical spectrum. The measured spectral linewidth at half maximum is about 730 kHz. The Lorentzian shapes generated by the beat notes between modes 1 and 2 and between modes 2 and 3 have the same spectral linewidths. This experiment demonstrates: 1) the SP in this DBR laser is an intra-cavity effect; 2) SP signal is composed of two beat notes with the same linewidths as the whole SP signal; and 3) the phases of modes 1 and 3 are identically correlated

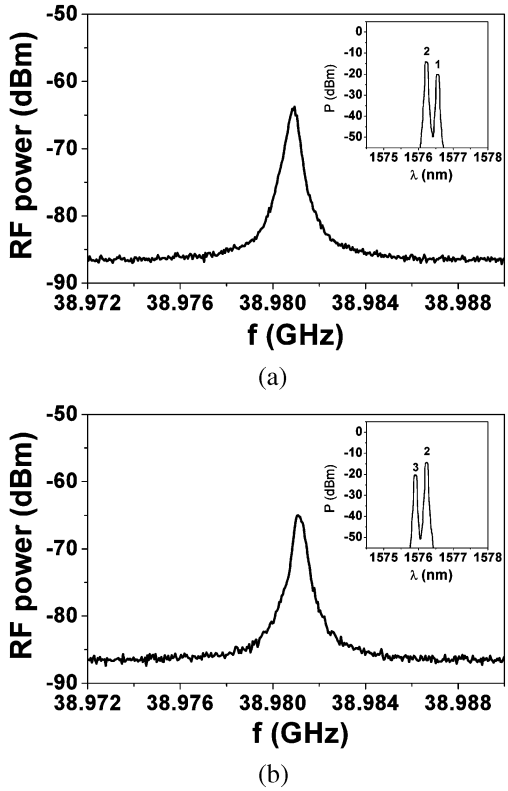

Fig. 9. Radio frequency spectra of (a) the beat note between modes 1 and 2 and (b) the beat note between modes 2 and 3. The inserts are the corresponding optical spectra.

to the phase of the mode 2. Therefore, since phase noise is the origin of spectral linewidth, such a result proves that the relative phases between adjacent modes have the same phase noise characteristics, suggesting that the modes are partly correlated under passive mode-locking (PML) operation.

The following section addresses a theoretical model developed to prove that FWM is largely responsible for phase synchronization under PML in DBR semiconductor lasers.

IV. Theoretical Model

The generation of SP at very high frequencies in a multimode semiconductor lasers can be associated with the well-known phenomenon of PML where modes are equally spaced and their relative phases are fixed. In the absence of a saturable absorber, PML can occur through non linear interactions between longitudinal modes that induce dynamic pulsation of both the gain and the refractive index. Considering the dependence of the carrier density on the optical power in semiconductor lasers, such dynamics originates from the sensitivity of the carrier density to the modulation of the optical power at the frequency of the mode beatings. In order to identify the origin of SP in DBR lasers, and in particular, to understand the observed phenomenon of phase correlation, a model, based on the time evolution of multiple optical fields generated inside the DBR laser, has been developed introducing a phase sensitive phenomenon: FWM. The contributions to FWM in multimode semiconductor lasers originate either from interband effects or from intraband effects. Intraband effects, resulting from carrier heating and spectral hole

burning, occur for mode spacings up to 1 THz, whereas interband effects, resulting from carrier density modulation, decrease above 1 GHz. Nevertheless, for mode spacings below 100 GHz, the magnitude of interband effects is still high compared to intraband effects, so that it is the dominant effect at 40 GHz. However, the model presented here can be easily generalized to take into account intraband effects.

A. Carrier Density Modulation

The DBR laser under study can be considered as a FP laser with one facet having a wavelength dependent reflectivity. According to the waveguide dimensions of the active section, the laser cavity supports only the fundamental TE mode with the transverse distribution $U(x,y)$. By considering that the reflectivities of the laser facets are sufficiently high, the longitudinal distribution of the optical field is assumed to be homogeneous. Such an approximation does not introduce significant errors when processing equations well above the threshold [18] and simplifies greatly the development of the multimode coupled rate equations. The monochromatic wave representing the optical field $E_k^{(c)}$ of the kth mode is then expressed as follows:

$$E_k^{(c)} = UE_k \exp(-\imath\omega_k t) \tag{1}$$

with the complex amplitude E_k defined as

$$E_k(t) = A_k(t)\exp\left(-\imath\phi_k(t)\right) \tag{2}$$

where A_k is the slowly time varying amplitude, ω_k is the locked angular frequency, and ϕ_k is the instantaneous phase fluctuation. In the case of a laser with M longitudinal modes, the total electric intensity is given by

$$|E_T|^2 = \sum_{k=1}^{M}|E_k|^2|U|^2 + \sum_{k=1}^{M}\sum_{l>k}^{M} E_kE_l^*|U|^2\exp(\imath\Omega_{lk}t) + \text{c.c.} \tag{3}$$

where c.c. denotes the complex conjugate of the proceeding term, and $\Omega_{lk} = \omega_l - \omega_k$. For a laser with two uncorrelated modes, a RF signal at the frequency $\Omega_{lk}/2\pi$ can be observed by a photodiode, with a spectral linewidth corresponding to the sum of the modes' spectral linewidths. In the SP regime, all modes generated inside the laser cavity are passively locked such that all mode-spacing angular frequencies are fixed to the so-called SP angular frequency Ω_{sp}. By setting $\Omega_{lk} = (l-k)\Omega_{\text{sp}} = m\Omega_{\text{sp}}$ in (3), the total light intensity can be rewritten as

$$|E_T|^2 = |E_{T0}|^2 + \sum_{m=1}^{M-1}\sum_{k=m+1}^{M} E_kE_{k-m}^*|U|^2\exp(-\imath m\Omega_{\text{sp}}t) + \text{c.c.} \tag{4}$$

with $|E_{T0}|^2$ being the time average photon density, corresponding to the first term of (3). This equation shows that the total light intensity contains the beating terms with several harmonics.

The origin of carrier density modulation (CDM) in DBR semiconductor lasers is then the interaction between the linear gain and the total optical field, as described by the carrier density rate equation below

$$\frac{dN}{dt} = \frac{I}{eV} - \frac{N}{\tau_e} - v_g g_d(N - N_{\text{tr}})\cdot|E_T|^2 \tag{5}$$

where the electric field E_T is scaled such that $|E_T|^2$ represents the photon density of the kth mode inside the laser cavity, I is the injected current in the gain medium, V is the volume of the active layer, e is the electron charge, τ_e is the carrier lifetime, v_g is the group velocity, g_d is the differential gain, and N_{tr} is the carrier density at transparency. The diffusion term has been ignored by assuming that transverse waveguide dimensions are smaller than the diffusion length. Moreover, the standing-wave effects can be neglected since spatial holes burned by counter-propagating waves are washed out by the carrier diffusion process in the longitudinal direction [19]. Considering that the carrier lifetime is longer that the intermode beating period, resolution of (5) is performed through a small signal analysis [20], [21] leading to a solution of the form

$$N = N_0 + \sum_{m=1}^{M-1}\left(N_m\exp(-\imath m\Omega_{\text{sp}}t) + \text{c.c.}\right) \tag{6}$$

with N_m being much smaller than N_0. By introducing (3) and (6) into (5), the following expression for the first order for N_m is found [22], [23]:

$$\begin{aligned} N_m &= |U|^2\Delta N_m \\ \Delta N_m &= -(N_0 - N_{\text{tr}})\cdot\frac{\sum_{k=m+1}^{M}E_kE_{k-m}^*/P_s}{1 + P_t/P_s - \imath m\Omega_{\text{sp}}\tau_e} \end{aligned} \tag{7}$$

with the photon saturation density $P_s = 1/(\Gamma v_g g_d \tau_e)$, and the local photon density $P_t = \sum_{k=1}^{M}|U|^2|E_k|^2$. Since $\Omega_{\text{sp}}\tau_e \gg 1$, the term $(1 + P_t/P_s)$ can be neglected compared to $m\Omega_{\text{sp}}\tau_e$. The spatial average carrier density $\overline{N}_0$, satisfies the following rate equation:

$$\frac{d\overline{N}_0}{dt} = \frac{I}{eV} - \frac{\overline{N}_0}{\tau_e} - G\overline{P}_t \tag{8}$$

where the overbar denotes averaging in spatial dimensions. $\overline{P}_t$ is the average photon density, G is the linear gain defined as $G = \Gamma v_g g_d(\overline{N}_0 - N_{\text{tr}})$, and Γ is the confinement factor.

B. Coupled Rate Equations

CDM leads to a nonlinear gain and refractive index modulation, affecting both the amplitude and the phase of the lasing modes. Corresponding to our experiments and for the sake of simplicity and clarity, only three longitudinal modes ($M = 3$) propagating in the SP DBR are considered in our approach. We start from rate equations of the kth passively locked mode for semiconductor lasers including the small-signal expression for the carrier density in (6) [20]

$$\begin{aligned} \frac{dE_k}{dt} &= \frac{1}{2}(1 - \imath\alpha_H)(G - \gamma_k) - \imath\left(\omega_k^i - \omega_k\right)E_k \\ &\quad + \frac{1}{2}(1 - \imath\alpha_H)v_g g_d\Gamma C \\ &\quad \times\left(\sum_{m=1}^{M-1}\left(\Delta N_m E_{k-m} + \Delta N_m^* E_{k+m}\right)\right) \end{aligned} \tag{9}$$

where α_H represents the phase-amplitude coupling factor, and γ_k the cavity losses for the kth mode. The linear gain G is assumed constant over the spectral range of the three modes. The occurrence of the term $(\omega_k - \omega_k^i)$ accounts for the detuning of

the locked angular frequency ω_k of the kth lasing mode from its cavity resonance one ω_k^i. C is the overlap factor, given by

$$C = \frac{\int_{-d/2}^{d/2}\int_{-w/2}^{w/2}|U|^4 dxdy}{\int_{-d/2}^{d/2}\int_{-w/2}^{w/2}|U|^2 dxdy}. \tag{10}$$

The overlap factor was first introduced by Bogatov [24] and Agrawal [20], and accounts for the influence of the transverse contribution to nonlinear gain.

Equation (9) is similar to those already developed by Sargent [25] and Shore [26] to describe mode-locking and coupling in multi-mode lasers. However, in our model, we concentrate on the effect of carrier density modulation resulting from the beating of longitudinal modes selected by the DBR mirror to determine the origin of SP. By separating the real and imaginary parts of (9), six rate equations are obtained, describing the time evolution of both the amplitude and the phase of the three modes:

$$\frac{dA_1}{dt} = \frac{G}{2}\left(1+\vartheta_{\rm cdm}\left(\frac{\alpha_H}{2}\frac{A_3^2}{P_s}+\alpha_H\frac{A_2^2}{P_s}+\sqrt{1+\alpha_H^2}\frac{A_2^2}{P_s}\frac{A_3}{A_1}\right.\right.$$
$$\left.\left.\times\sin(\psi+\arctan\alpha_H)\right)\right)A_1-\frac{\gamma_1}{2}A_1 \tag{11}$$

$$\frac{dA_2}{dt} = \frac{G}{2}\left(1-\vartheta_{\rm cdm}\alpha_H\left(\frac{A_1^2}{P_s}-\frac{A_3^2}{P_s}\right)\right)A_2-\frac{\gamma_2}{2}A_2 \tag{12}$$

$$\frac{dA_3}{dt} = \frac{G}{2}\left(1-\vartheta_{\rm cdm}\left(\frac{\alpha_H}{2}\frac{A_1^2}{P_s}+\alpha_H\frac{A_2^2}{P_s}+\sqrt{1+\alpha_H^2}\frac{A_2^2}{P_s}\frac{A_1}{A_3}\right.\right.$$
$$\left.\left.\times\sin(\psi+\arctan\alpha_H)\right)\right)A_3-\frac{\gamma_3}{2}A_3 \tag{13}$$

$$\frac{d\phi_1}{dt} = \left(\omega_1-\omega_1^i\right)+\frac{G}{2}\left(\alpha_H-\vartheta_{\rm cdm}\left(\frac{1}{2}\frac{A_3^2}{P_s}+\frac{A_2^2}{P_s}+\sqrt{1+\alpha_H^2}\frac{A_2^2}{P_s}\frac{A_3}{A_1}\right.\right.$$
$$\left.\left.\times\cos(\psi+\arctan\alpha_H)\right)\right)-\frac{\gamma_1}{2} \tag{14}$$

$$\frac{d\phi_2}{dt} = \left(\omega_2-\omega_2^i\right)+\frac{G}{2}\left(\alpha_H+\vartheta_{\rm cdm}\left(\frac{A_1^2}{P_s}-\frac{A_3^2}{P_s}\right)\right)-\frac{\gamma_2}{2} \tag{15}$$

$$\frac{d\phi_3}{dt} = \left(\omega_3-\omega_3^i\right)\frac{G}{2}\left(\alpha_H+\vartheta_{\rm cdm}!\left(\frac{1}{2}\frac{A_1^2}{P_s}+\frac{A_2^2}{P_s}+\sqrt{1+\alpha_H^2}\frac{A_2^2}{P_s}\frac{A_1}{A_3}\right.\right.$$
$$\left.\left.\times\cos(\psi+\arctan\alpha_H)\right)\right)-\frac{\gamma_3}{2} \tag{16}$$

where $\vartheta_{\rm cdm}$ quantifies the effect of carrier density modulation, and ψ is the relative phase mismatch defined, respectively, as

$$\vartheta_{\rm cdm} = \frac{C}{\Omega_{\rm sp}\tau_e} \qquad \psi = (\phi_2-\phi_1)-(\phi_3-\phi_2). \tag{17}$$

We can see that amplitude and phase rate equations do not depend on individual phases but on the relative phase mismatch. We also observe the addition of non linear terms, expressing either energy or phase transfers between modes. The nonlinear phase-independent terms lead to the gain enhancement of mode 1 and gain reduction of the mode 3. The nonlinear phase sensitive terms depends on the relative phase mismatch ψ. It is noted that, considering three longitudinal modes in the laser, only beatings at the fundamental pulsation may induce phase transfers. This is the reason why no term of phase transfer appears in the rate equation of the center field E_2.

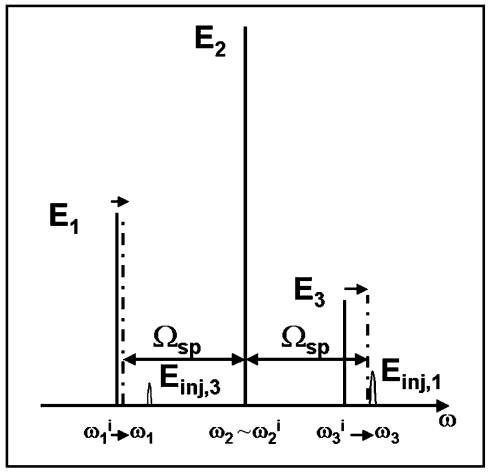

Fig. 10. Schematic description of mutual injection regime through modulation side bands from FWM, leading to passively modes locked at $\Omega_{\rm sp} \sim \omega_2 - \omega_1$.

C. Mutual Injection Locking and Locking Bandwidth

The beating process among longitudinal modes modulates the carrier density at multiples of the mode-spacing frequencies. The latters vary from one pair of modes to the other in the DBR laser because of the dispersion of the effective length in the Bragg grating. The self-induced carrier density pulsation leads to cross-saturation and FWM through the creation of dynamic index and gain gratings, and generates modulation sidebands that act as optical injection signals for modes, as shown in Fig. 10. This effect appears to be a mutual injection-locking phenomenon that reaches equilibrium when all mode-spacing frequencies are locked to the same value $\Omega_{\rm sp}$ with appropriate power distribution among modes.

To provide more insight into the mechanism of mutual injection locking, let us introduce the injection optical fields $E_{\rm inj,1}$ and $E_{\rm inj,3}$ explicitly expressed by

$$E_{\rm inj,1} = \rho_{\rm inj,1}\cdot\exp(\phi_{\rm inj,1})$$
$$E_{\rm inj,3} = \rho_{\rm inj,3}\cdot\exp(\phi_{\rm inj,3})$$

with the injection rate $\rho_{\rm inj,k}$ and the phase $\phi_{\rm inj,k}$, respectively, defined as

$$\rho_{\rm inj,1} = G\vartheta_{\rm cdm}\sqrt{1+\alpha_H^2}\frac{A_2^2}{P_s}\frac{A_1}{A_3}$$
$$\rho_{\rm inj,3} = G\vartheta_{\rm cdm}\sqrt{1+\alpha_H^2}\frac{A_2^2}{P_s}\frac{A_3}{A_1}$$

and

$$\phi_{\rm inj,1} = 2\phi_2-\phi_1+\arctan\alpha_H$$
$$\phi_{\rm inj,3} = 2\phi_2-\phi_3+\arctan\alpha_H.$$

These terms describe the injection of optical fields of amplitude $(A_2^2/P_s)A_k$ ($k = \{1,3\}$) balanced by the magnitude of the non linear effects $G\vartheta_{\rm cdm}\sqrt{1+\alpha_H^2}$. Introducing injection

rate terms in the couled rate (11)–(16), we achieve the following equations for the amplitudes and the phases:

$$\frac{dA_1}{dt} = \frac{G}{2}\left(1+\vartheta_{\rm cdm}\left(\frac{\alpha_H}{2}\frac{A_3^2}{P_s}+\alpha_H\frac{A_2^2}{P_s}\right)\right)A_1 + \frac{\rho_{\rm inj,3}}{2}\sin(\phi_{\rm inj,3}-\phi_1)A_1 - \frac{\gamma_1}{2}A_1 \quad (18)$$

$$\frac{dA_2}{dt} = \frac{G}{2}\left(1-\vartheta_{\rm cdm}\alpha_H\left(\frac{A_1^2}{P_s}-\frac{A_3^2}{P_s}\right)\right)A_2 - \frac{\gamma_2}{2}A_2 \quad (19)$$

$$\frac{dA_3}{dt} = \frac{G}{2}\left(1-\vartheta_{\rm cdm}\left(\frac{\alpha_H}{2}\frac{A_1^2}{P_s}+\alpha_H\frac{A_2^2}{P_s}\right)\right)A_3 - \frac{\rho_{\rm inj,1}}{2}\sin(\phi_{\rm inj,1}-\phi_3)A_3 - \frac{\gamma_3}{2}A_3 \quad (20)$$

$$\frac{d\phi_1}{dt} = (\omega_1-\omega_1^i)+\frac{G}{2}\left(\alpha_H-\vartheta_{\rm cdm}\left(\frac{1}{2}\frac{A_3^2}{P_s}+\frac{A_2^2}{P_s}\right)\right) - \frac{\rho_{\rm inj,3}}{2}\cos(\phi_{\rm inj,3}-\phi_1)-\frac{\gamma_1}{2} \quad (21)$$

$$\frac{d\phi_2}{dt} = (\omega_2-\omega_2^i)+\frac{G}{2}\left(\alpha_H+\vartheta_{\rm cdm}\left(\frac{A_1^2}{P_s}-\frac{A_3^2}{P_s}\right)\right)-\frac{\gamma_2}{2} \quad (22)$$

$$\frac{d\phi_3}{dt} = (\omega_3-\omega_3^i)+\frac{G}{2}\left(\alpha_H+\vartheta_{\rm cdm}\left(\frac{1}{2}\frac{A_1^2}{P_s}+\frac{A_2^2}{P_s}\right)\right) + \frac{\rho_{\rm inj,1}}{2}\cos(\phi_{\rm inj,1}-\phi_3)-\frac{\gamma_3}{2}. \quad (23)$$

The two pairs of (18) and (21) and (20) and (23) for side modes are similar to those describing an externally injection-locked laser [27]. The only difference with external injection locking phenomenon is that the injection optical fields are self-generated inside the laser cavity. These equations really demonstrate that modulation side bands created by FWM act as an internal injection signal. Fig. 10 shows schematically the mutual injection locking process. For the sake of simplicity, ω_2 is considered equal to ω_2^i in this schematic description. The effect of the modulation side-bands depends on the relative power between the modes involved (1 and 3 here) through the injection rate terms. Indeed, the stronger the modulation side-band, the larger the frequency shift of the injected mode. This is the reason why the SP frequency is approximately the mode-spacing frequency between the two main modes. Since this phenomenon of mutual injection locking enables the shift of modes' angular frequency from cavity resonance to match the condition for modes passively locked ($\omega_3-\omega_2=\omega_2-\omega_1=\Omega_{\rm sp}$), our modeling of PML including CDM is self-consistent.

D. Steady-State Analysis

In order to determine the validity limit of this system of differential (11)–(16), the time-rate of change of amplitudes and phases are set to zero. Time variables of amplitude and phase are substituted by their static values written A_k^0 and ϕ_k^0. The stationary equations leads to a relation between the relative phase mismatch, ψ^0, and initial angular frequency mismatch, $\Delta\omega^i$ defined as $(\omega_2^i-\omega_1^i)-(\omega_3^i-\omega_2^i)$. Under the SP condition $(\omega_2-\omega_1=\omega_3-\omega_2)$, we obtain the following expression of initial angular frequency mismatch:

$$\Delta\omega^i = \frac{\sqrt{1+\alpha_H^2}}{2}(\rho_{\rm inj,1}-\rho_{\rm inj,3})\left(\frac{3}{2}\frac{A_3^0A_1^0}{A_2^{0^2}}-\cos(\psi^0)\right).$$

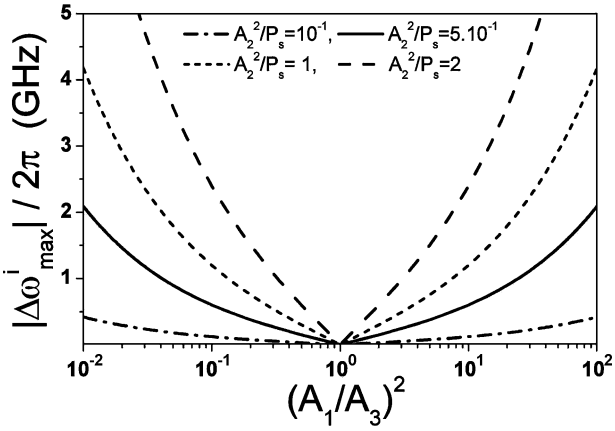

Fig. 11. Evolution of the maximum initial frequency mismatch $\Delta\nu^i$ versus the injection power rate, for different values of the ratio A_2^2/P_s.

This expression again shows the consistency of the model because the introduction of FWM leads to a stationary value of the relative phase mismatch, which is a necessary condition for the PML regime. The relative phase mismatch ψ^0, which determines the temporal profile of the SP output power [28], is related to the initial angular frequency mismatch induced by the dispersion of the Bragg grating, which is cancelled out by FWM. By the way, (24) gives a limit value of the initial angular frequency mismatch that can be cancelled out by FWM to achieve PML

$$|\Delta\omega^i| < \frac{5}{4}\sqrt{1+\alpha_H^2}|\rho_{\rm inj,1}-\rho_{\rm inj,3}|. \quad (24)$$

When the initial angular frequency mismatch $\Delta\omega^i$ exceeds this limit value, passive mode-locking cannot be achieved. Such a limit is similar to the locking bandwidth, defined for external optical injection, and is fixed by the injection rate terms [27]. The phase-amplitude coupling factor may also induce an enhancement of the maximal detuning between initial frequencies. Furthermore, when one of the side modes is stronger than the other, the locking strength increases to induce a larger frequency shift of the other side mode, as shown in Fig. 11. This figure also shows that, by increasing the photon density inside the cavity (expressed by the ratio A_2^2/P_s), the locking bandwidth quickly becomes larger than 100 MHz for any injection power rate. Considering a free spectral range in the order of 40 GHz for our DBR lasers, such values of locking bandwidth explains why SP appears as soon as the output power reaches 1 mW in our DBR laser. Therefore, such a result demonstrates that SP at 40 GHz is easily achieved in DBR semiconductor lasers because interband effects are sufficiently important to induce a natural occurrence of PML at typical power levels as it is shown by Fig. 5.

E. Calculations of Frequency Noise Spectral Densities

The instantaneous fluctuations of the electric fields, due to spontaneous emission, induce amplitude and phase fluctuations around their static values. The study of the phase noise characteristic, which is essential to investigate phase correlation, requires taking such fluctuations into account in our rate equations using Langevin noise sources F_{A_k}, F_{ϕ_k}, and F_N, respectively, for amplitude, phase and carrier density. These Langevin

TABLE I
PARAMETERS USED FOR CALCULATIONS

Parameters & Unit	Symbols	Values
Width $[m]$	w	1.5×10^{-6}
Thickness $[m]$	d	0.3×10^{-6}
Total length $[m]$	L	1.15×10^{-3}
Linewidth enhancement factor	α_H	4
Optical confinement factor	Γ	0.1
Overlap factor	C	0.8
Gain group index	n_g	4
Phase and Bragg group indices	n_φ, n_B	3.3
Carrier lifetime $[s]$	τ_e	1.7×10^{-9}
Carrier density at transparency $[m^{-3}]$	N_{tr}	1×10^{24}
Differential gain $[m^2]$	a	9×10^{-20}
Total material losses $[cm^{-1}]$	γ_{int}/v_g	15
Spontaneous emission rate $[s^{-1}]$	R_{sp}	2×10^{12}
Self-pulsation frequency $[GHz]$	$\Omega_{sp}/2\pi$	40

sources are characterized by their spectral densities as follows [29], [30]:

$$\left\langle \widetilde{F}_{A_k}(\Omega) \cdot \widetilde{F}^*_{A_k}(\Omega') \right\rangle = \frac{R_{\rm sp}}{2} \cdot \delta(\Omega - \Omega') \tag{25}$$

$$\left\langle \widetilde{F}_{\phi_k}(\Omega) \cdot \widetilde{F}^*_{\phi_k}(\Omega') \right\rangle = \frac{R_{\rm sp}}{2A_k^{0^2} V} \cdot \delta(\Omega - \Omega') \tag{26}$$

$$\left\langle \widetilde{F}_N(\Omega) \cdot \widetilde{F}^*_N(\Omega') \right\rangle = \frac{I}{eV} \cdot \delta(\Omega - \Omega') \tag{27}$$

where $R_{\rm sp}$ is the spontaneous emission rate, $\delta(\Omega)$ is the Dirac distribution, and $\widetilde{X}$ denotes the Fourier Transform of the variable X. After linearization and Fourier transformation of (9), (11)–(16), including the Langevin noise sources, the following equation is achieved for the angular analysis frequency Ω:

$$(j\Omega I - M) \cdot \begin{pmatrix} \delta\widetilde{A}_1 \\ \delta\widetilde{A}_2 \\ \delta\widetilde{A}_3 \\ \delta\widetilde{\phi}_1 \\ \delta\widetilde{\phi}_2 \\ \delta\widetilde{\phi}_3 \\ \delta\widetilde{N}_0 \end{pmatrix} = \begin{pmatrix} \widetilde{F}_{A_1} \\ \widetilde{F}_{A_2} \\ \widetilde{F}_{A_3} \\ \widetilde{F}_{\phi_1} \\ \widetilde{F}_{\phi_2} \\ \widetilde{F}_{\phi_3} \\ \widetilde{F}_N \end{pmatrix} \tag{28}$$

where M is a 7×7 matrix and I the unity matrix. For any values of Ω satisfying the condition that $\det(j\Omega I - M) \neq 0$, we can express the phase fluctuations of the three modes as a function of the Langevin terms. Writing

$$Q = (j\Omega I - M)^{-1} = (q_{ij})_{\{i,j\}\varepsilon[1,6]} \tag{29}$$

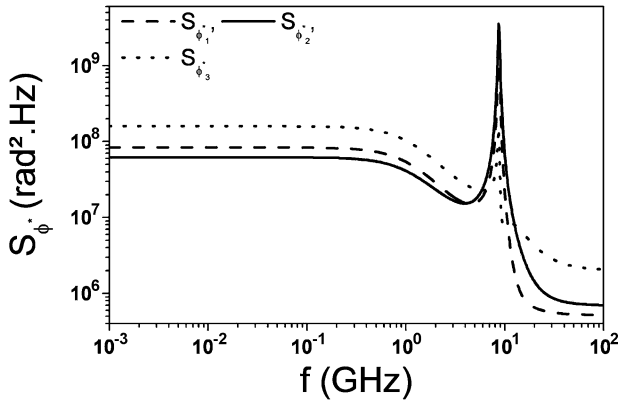

Fig. 12. Numerical calculations of FM noise spectra for longitudinal modes.

the phase fluctuations are given directly by

$$\delta\widetilde{\phi}_k(\Omega) = \sum_{i=1}^{7} q_{k+3,i} \widetilde{F}_i(\Omega) \tag{30}$$

where k varies from 1 to 3, q are the elements of matrix Q, and $\widetilde{F}_i$ is equal to $\widetilde{F}_{A_i}$ for $i = 12, 3,$, $\widetilde{F}_{\phi_i}$ for $i = 4, 5, 6$, and $\widetilde{F}_N$ for $i = 7$. Using (30) and the properties of the Langevin sources, the power spectral density (PSD) of the phase noise of the kth mode can be written as follows:

$$S_{\phi_k}(\Omega) = \left\langle \delta\widetilde{\phi}_k(\Omega) \cdot \delta\widetilde{\phi}^*_k(\Omega) \right\rangle \tag{31}$$

$$= \sum_{i=1}^{7} |q_{k,i}|^2 \left\langle \widetilde{F}_i(\Omega) \cdot \widetilde{F}^*_i(\Omega) \right\rangle. \tag{32}$$

The PSD of frequency modulation (FM) noise can then be obtained using the following relation:

$$S_{\dot{\phi}_k}(\Omega) = \Omega^2 S_{\phi_k}(\Omega). \tag{33}$$

In our numerical calculations, the steady operating points are first obtained by the Runge–Kutta method. The values of parameters used for these calculations are listed in Table I. Fig. 12 shows the PSD of FM noise of the three individual modes as a function of analysis frequency $f = \Omega/2\pi$ for an injected active current equal to ten times the threshold current. We observe a relaxation oscillation peak at a frequency of 9 GHz for the modes. Assuming a Lorentzian shape for longitudinal modes, the spectral linewidth is given by $S_{\dot{\phi}_k}(0)/2\pi$, yielding spectral linewidths of tens of megahertz. Then, we calculated the PSD of relative phases ϕ_{21} and ϕ_{32} by using the relation

$$S_{\dot{\phi}_{lk}}(\Omega) = \Omega^2 S_{\phi_{lk}}(\Omega). \tag{34}$$

Fig. 13 shows the FM noise PSD of the relative phases, and the sum of FM noise PSD for longitudinal modes, for the same biasing conditions as in Fig. 12. The solid curves describe the FM noise spectra related to the beating between modes 1 and 2, and the dashed ones describe the FM noise spectra related to the

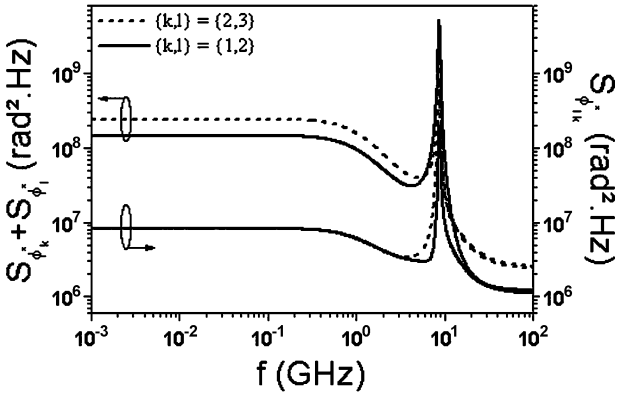

Fig. 13. Numerical calculations of FM noise spectra for the relative phases ϕ_{21} and ϕ_{32} compared to the sum of FM noise spectra for longitudinal modes.

beating between modes 2 and 3. We observe a large reduction of PSD of the relative phases from that of the sum of FM noise PSD of the longitudinal modes for low analysis frequencies. The calculated values of the spectral linewidths are of the same order as those observed experimentally. More importantly, these theoretical values are identical for ϕ_{21} and ϕ_{32} in a range of several tens of MHz around the analysis frequency, which shows that the correlation level between the phases of modes 1 and 2 is the same as that between the phases of modes 2 and 3. This completely agrees with experimental results in Fig. 9(a) and (b) showing that the modes are identically correlated in phase due to FWM.

F. Discussion on the Spectral Linewidth Reduction

As was observed experimentally and theoretically, SP is characterized by a large reduction of the RF spectral linewidth compared to the linewidths of the optical modes involved in the beating process. This reduction of the phase fluctuations is attributed to the combination of two major effects. First, optical phase noise is principally associated with two processes driven by spontaneous emission: direct phase fluctuations, and additional phase fluctuations arising from carrier fluctuations. Whereas the first process is specific to each optical mode, the second one is actually common to all modes [31]. Indeed, as described by Henry [32] in the case of single mode lasers, spontaneous emission leads to intensity fluctuations of modes followed by gain fluctuations in order to return to their equilibrium values. The carrier density fluctuations then induce index fluctuations through the phase-amplitude coupling process [33], which gives rise to additional phase fluctuations. In multimode DBR lasers, with small spectral range, the linear gain is nearly identical for all modes so that these additional phase fluctuations are common to all modes. This phenomenon is actually demonstrated by Fig. 8. Despite large power differences between the dominant mode and the other ones, the linewidth enhancements of these modes are very close, showing that the modes are not independent. Therefore, the beating process that gives rise to SP naturally suppresses common phase fluctuations arising from this second process. Such a phenomenon induces a SP spectral linewidth narrower than that of the optical modes. Moreover, as discussed in the previous section, another effect is superimposed to this one: the effect of FWM. Consequently, the reduction of SP spectral linewidth results from the combined effects of FWM and of the cancellation of common phase fluctuations due to the beating process.

V. Conclusions

In this paper, SP in DBR lasers was analyzed experimentally and theoretically. A detailed characterization of the component was presented. The origin of the SP in such components has been clearly identified: the carrier modulation resulting from the beating of adjacent longitudinal modes selected by the DBR mirror. The theoretical work based on the rate equations for three modes has been developed to study the time evolution of the phases and amplitudes of the passively locked modes. We proved that FWM is responsible for mutual injection locking between lasing modes. We also demonstrated, experimentally and theoretically, that the phases of the longitudinal modes are identically correlated through the FWM in this type of SP lasers. Our analysis can satisfactorily explain the experimental results obtained from these lasers, and provide guidelines for the design of high-performance SP DBRs for 40-Gbit/s all-optical clock recovery as well as optical microwave sources for radio-over-fiber and RADAR applications.

References

[1] A. Jourdan, "The perspective of optical packet switching inIP dominant backbone and metropolitan networks," *IEEE Commun. Mag.*, vol. 39, pp. 136–141, 2001.

[2] B. Lavigne, P. Guerber, P. Brindel, E. Balmefrezol, and B. Dagens, "Cascade of 100 optical 3R regenerators at 40 Gbit/s based on all-active Mach–Zehnder interferometer," presented at the Eur. Conf. Opt. Commun. (ECOC), 2001, paper We.F.2.6.

[3] L. F. Tiemeijer, P. I. Kuindersma, P. J. A. Thijs, and G. L. J. Rikken, "Passive FM locking in InGaAsP semiconductor lasers," *IEEE J. Quantum Electron.*, vol. 25, no. 6, pp. 1385–1392, Jun. 1989.

[4] K. Sato, "Optical pulse generation using Fabry–Perot lasers under continuous wave operation," *IEEE J. Sel. Topics Quantum Electron.*, vol. 9, no. 5, pp. 1288–1293, Sep./Oct. 2003.

[5] M. Mohrle, B. Sartorius, R. Steingruber, and P. Wolfram, "Electrically switchable self-pulsations in integratable multisection DFB-lasers," *IEEE Photon. Technol. Lett.*, vol. 8, no. 1, pp. 28–30, Jan. 1996.

[6] W. Mao, Y. Li, M. Al-Mumin, and G. Li, "All-optical clock recovery from RZ-format data by using a two-section gain-coupled DFB laser," *J. Lightw. Technol.*, vol. 20, no. 9, pp. 1705–1714, Sep. 2002.

[7] S. Arahira, S. Oshiba, Y. Matsui, T. Kunii, and Y. Ogawa, "500 GHz optical short pulse generation from a monolithic passively mode-locked distributed Bragg reflector laser diode," *Appl. Phys. Lett.*, vol. 64, no. 15, pp. 1917–1919, 1994.

[8] T. Ohno, R. Iga, Y. Kondo, T. Ito, T. Futura, H. Ito, and K. Sato, "Wide-locking-range 160-GHz optical clock recovery from 160-Gbit/s signal using mode-locked laser diode," presented at the Opt. Fiber Commun. Conf. 2004, Los Angeles, CA, 2004, paper WD5.

[9] M. Mohrle, B. Sartorius, C. Bornholdt, S. Bauer, O. Brox, A. Sigmund, R. Steingruber, H. Radziunas, and H.-J. Wunsche, "Detuned grating multisection-RW-DFB lasers for high-speed optical signal processing," *IEEE J. Sel. Topics Quantum Electron.*, vol. 7, pp. 217–223, 2001.

[10] O. Brox, S. Bauer, M. Biletzke, H. Ding, J. Kreissl, H.-J. Wunsche, and B. Sartorius, "Self-pulsating DFB for 40 GHz clock-recovery: impact of intensity fluctuations on jitter," presented at the Optical Fiber Commun. Conf., Los Angeles, CA, 2004, paper MF55.

[11] Y. Li, C. Kim, G. Li, Y. Kaneko, R. L. Jungerman, and O. Buccafusca, "Wavelength and polarization insensitive all-optical clock recovery from 96 Gb/s data by using a two-section gain-coupled DFB laser," *IEEE Photon. Technol. Lett.*, vol. 15, no. 4, pp. 590–592, Apr. 2003.

[12] H. Bao, Y. J. Wen, and H. F. Liu, "Impact of saturable absorption on performance of optical clock recovery using a mode-locked multisection semiconductor laser," *IEEE J. Quantum Electron.*, vol. 40, no. 9, pp. 1177–1185, Sep. 2004.

[13] G.-H. Duan, C. Gosset, B. Lavigne, R. Brenot, B. Thedrez, J. Jacquet, and O. Leclerc, "40 GHz all-optical clock recovery using polarization insensitive distributed Bragg reflector lasers," presented at the CLEO, Baltimore, MD, 2003, paper CThQ5.
[14] P. Landais, J. Renaudier, P. Gallion, and G.-H. Duan, M. Osinski, H. Amano, and F. Henneberger, Eds., "Analysis of self-pulsation in distributed Bragg reflector laser based on four-wave mixing," *Proc. SPIE*, vol. 5349, pp. 262–270, 2004.
[15] P. Bardella and I. Montrosset, "Analysis of self-pulsating three-section DBR lasers," *IEEE J. Sel. Topics Quantum Electron.*, vol. 11, no. 2, pp. 361–366, Mar./Apr. 2005.
[16] Y. Suematsu, S. Arai, and K. Kishino, "Dynamic single-mode semiconductor lasers with a distributed reflector," *J. Lightw. Technol.*, ser. 1, vol. LT-1, pp. 161–176, Mar. 1983.
[17] H.-F. Liu, S. Arahira, T. Kunii, and Y. Ogawa, "Tuning characteristics of monolithic passively mode-locked distributed Bragg reflector semiconductor lasers," *IEEE J. Quantum Electron.*, vol. 32, no. 11, pp. 1965–1975, Nov. 1996.
[18] G. P. Agrawal and N. K. Dutta, *Semiconductor Lasers*, 2nd ed. Norwell, MA: Kluwer, 1993, ch. 6.
[19] G. P. Agrawal, "Highly nondegenerate four-wave mixing in semiconductor lasers due to spectral hole burning," *Opt. Lett.*, vol. 12, no. 4, pp. 260–262, 1987.
[20] ——, "Population pulsations and nondegenerate four-wave mixing in semiconductor lasers and amplifiers," *J. Opt. Soc. Amer. B*, vol. 5, no. 1, pp. 302–304, 1988.
[21] M. Yamada, "Theoretical analysis of nonlinear optical phenomena taking into account the beating vibration of the electron density in semiconductor lasers," *J. Appl. Phys.*, vol. 66, pp. 81–89, 1989.
[22] G. R. Gray and G. P. Agrawal, "Importance of self-induced carrier-density modulation in semiconductor lasers," *IEEE Photon. Technol. Lett.*, vol. 4, no. 11, pp. 1216–1219, Nov. 1992.
[23] A. Godard, G. Pauliat, G. Roosen, P. Graindorge, and P. Martin, "Side-mode gain in grating-tuned extended-cavity semiconductor lasers: investigation of stable single mode operation conditions," *IEEE J. Quantum Electron.*, vol. 38, no. 4, pp. 390–401, Apr. 2002.
[24] A. P. Bogatov, P. G. Eliseev, and B. N. Sverdlov, "Anomalous interaction of spectral modes in a semiconductor laser," *IEEE J. Quantum Electron.*, vol. 11, no. 7, pp. 510–515, Jul. 1975.
[25] M. Sargent, III, M. P. Scully, and W. E. Lamb, *Laser Physics*. Reading, MA, USA: Addison Wesley, 1974.
[26] K. A. Shore and W. M. Yee, "Theory of self-locking FM operation in semiconductor lasers," *Proc. Inst. Elect. Eng.*, vol. 138, no. 2, pp. 91–96, 1991.
[27] I. Petitbon, P. Gallion, G. Debarge, and C. Chabran, "Locking bandwidth and relaxation oscillation of an injection-locked semiconductor laser," *IEEE J. Quantum Electron.*, vol. 24, no. 2, pp. 148–154, Feb. 1988.
[28] C. Gosset, J. Renaudier, G.-H. Duan, G. Aubin, and J.-L. Oudar, "Phase and amplitude characterization of a 40 GHz self-pulsating DBR laser based on autocorrelation analysis," *J. Lightw. Technol.*, vol. 24, no. 2, pp. 970–975, Feb. 2006.
[29] C. H. Henry, "Theory of spontaneous emission noise in open resonators and its application to lasers and optical amplifiers," *J. Lightw. Technol.*, vol. 4, no. 3, pp. 288–297, Mar. 1986.
[30] P. Spano, S. Piazzolla, and M. Tamburrini, "Phase noise in semiconductor lasers: a theoretical approach," *IEEE J. Quantum Electron.*, vol. 19, no. 7, pp. 1195–1199, Jul. 1983.
[31] R. H. Wentworth, "Noise of strongly-raultimode laser diodes used in interferometric systems," *IEEE J. Quantum Electron.*, vol. 26, no. 3, pp. 426–442, Mar. 1990.
[32] C. H. Henry, "Theory of the phase noise and power spectrum of a single mode injection laser," *IEEE J. Quantum Electron.*, vol. 19, no. 9, pp. 1391–1397, Sep. 1983.
[33] ——, "Theory of the linewidth of semiconductor lasers," *IEEE J. Quantum Electron.*, vol. 18, no. 2, pp. 259–264, Feb. 1982.

Jeremie Renaudier was born in Laval, France, on October 27, 1978. He received the B.S. degree from the Ecole Nationale Supérieure des Télécommunications (ENST-Bretagne), Brest, France, the M.S. degree in optical communications and networks from the University de Bretagne Occidentale, Brest, France, both in 2002, and the Ph.D. degree from the Ecole Nationale Supérieure des Télécommunications (ENST), Paris, France, in 2006. His Ph.D. thesis, carried out at Alcatel Thales III-V Lab and ENST, was focused on the functional mode-locked DBR lasers for telecommunications applications at 40 Gb/s and beyond.

He is now with Alcatel Research & Innovation, Marcoussis, France, working on optical transmission systems.

Guang-Hua Duan (S'88–M'90–SM'01) received the B.E. degree from Xidian University, Xi'an, China, in 1983, and the M.E. and Ph.D. degrees, both from the Ecole Nationale Supérieure des Télécommunications (ENST), Paris, France, in 1987 and 1991, respectively, all in applied physics. He was habilitated to direct researches by the Université de Paris-Sud, Paris, France, in 1995.

He is now the Leader of the team "Lasers for Telecommunication Applications" within Alcatel Thales III-V Laboratory, Palaiseau, France, with research activities on nanophotonics, advanced semiconductor lasers, optical amplifiers, and functional optoelectronic subsystems for core and metro networks. Previously, he was a Postdoctoral Fellow supported by both Alcatel Alsthom Research and ENST from 1991 to 1992. Then, he was an Assistant, then an Associate Professor at ENST from 1992 to 2000. He was with the University of Maryland, College Park, as a Visiting Associate Professor from 1998 to 1999. He joined Opto+, Alcatel Research & Innovation Center, Marcoussis, in October 2000. He is the author or coauthor of more than 150 research papers, eight patents, and a contributor to book chapters. He lectures in the fields of electromagnetism, optoelectronics, and laser physics at ENST and at Ecole Superieure d'Optique.

Pascal Landais (M'02) received the Ph.D. degree in applied physics from the Ecole Nationale Supérieure des Télécommunications, Paris, France, in 1995, where he studied bistable and self-pulsating semiconductor lasers as all-optical functional components in fiber telecommunication systems.

In 1996, he joined the Physics Department, Trinity College, Dublin, Ireland, where he developed low-coherence semiconductor lasers for data storage and stabilized Fabry–Perot lasers. Between 1997 and 1999, he was involved in research activities on microcavity light-emitting diodes under the European project SMILED. Between 1999 and 2000, he was a Development Manager in CeramOptec Ltd., Ireland. Since January 2001, he has been a Lecturer in the School of Electronic Engineering, Dublin City University, Dublin, Ireland, where he has since developed, and currently directs research on, components for optical communication systems and terahertz generation. His group is part of the Research Institute for Networks and Communications Engineering, known as RINCE.

Dr. Landais is a TMR Marie Curie Fellow.

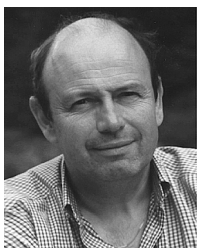

Philippe Gallion (M'82–SM'93) received the "Doctorat de Troisìme Cycle" from the University of Reims, France, in 1975 and the "Doctorat d'Etat" from the University of Montpellier, Frnace, in 1986.

In 1978, he joined the Ecole Nationale Supérieure des Télécommunications (ENST) where he is presently a Full Professor. He is carrying out research at the Laboratoire de Traitement et Communication de l'Information, (LTCI), joint research laboratories between ENST and the Centre National de la Recherche Scientifique (CNRS), where he is in charge of research activities in the fields of communications, electronics, radio-frequencies and optoelectronics. He has made pioneering contributions on laser noise, injection locking, semiconductor laser modulation chirp and tuning, coherent systems and optical devices, digital optical communications systems and networks. His present research topics include theory, design, modelling and characterization of functional devices, advanced optical digital communication systems and networks, radio over fiber systems, and quantum cryptography systems. He is author or coauthor of more than 180 technical papers and communications and he has served as advisor for more than 40 Ph.D. degree thesis.

Dr. Gallion is a member of the Optical Society of America. He is the Chairman of the IEEE Laser and Electro Optics Society (LEOS) French Chapter. He serves on the Editorial Board and Scientific Committee of several technical publications and as member of program or steering committee of international scientific meetings.